Available online at www.sciencedirect.com
SCIENCE DIRECT®
Geochimica et Cosmochimica Acta 70 (2006) 3970–3985
Geochimica
www.elsevier.com/locate/gca

A synthetic fluid inclusion study of copper solubility in hydrothermal brines from 525 to 725 °C and 0.3 to 1.7 GPa

Alistair C. Hack [a,*], John A. Mavrogenes [a,b]

[a] Research School of Earth Sciences, The Australian National University, Canberra, ACT 0200, Australia
[b] Department of Earth and Marine Sciences, The Australian National University, Canberra, ACT 0200, Australia

Received 18 August 2005; accepted in revised form 19 April 2006

Abstract

Fluid inclusions were synthesized in a piston-cylinder apparatus under mineral-buffered conditions over a range of Cl concentration (0.29 to 11.3 mol kg^{-1}), temperature (525 to 725 °C), and pressure (0.3 to 1.7 GPa). All fluids were buffered by the mineral assemblage native copper + cuprite + talc + quartz. In situ fluid composition was determined by analysing individual fluid inclusions by LA-ICPMS and independently analysing the quench solution. The solubility data provide basic information necessary to model the high temperature behaviour of Cu in magmatic-hydrothermal systems. Copper concentrations up to ~15 wt% were measured at 630 °C and 0.34 GPa. These results give an upper limit for Cu in natural fluids and support field-based observations of similar high Cu concentrations in fluids at near-magmatic conditions. Experimental evidence indicates that Cu^{+} may form neutral chloride complexes with the general stoichiometry $CuCl(HCl)^{0}_{n-1}$ with n up to 4, though $n \leqslant 2$ is typical for the majority of the experimental conditions. At high pressure (>~0.5 GPa) there is evidence that hydroxide species, e.g., $CuOH^{0}$, become increasingly important and may predominate over copper(I)-chloride complexes. The roles of fluid mixing, cooling and decompression in ore-forming environments are also discussed.

1. Introduction

The majority of economic copper deposits are hydrothermal in origin and often display an intimate spatial and temporal association with shallow-level igneous rocks at the deposit- and regional-scales in subduction-related, magmatic arc settings (e.g., Gustafson and Hunt, 1975; Dilles, 1987; Stoffregen, 1987; Hedenquist et al., 1993; Ulrich et al., 1999, 2001). Depending upon the depth of formation and style of mineralisation, these deposits are commonly referred to as porphyry (~1 to 3 km depth) or epithermal systems (<~1 km). Numerous petrological, isotopic and geochemical studies have established that ore-metals in porphyry-epithermal systems were originally scavenged from silicate melt by aqueous fluids that exsolved from the parent magma (e.g., Sheppard et al., 1969, 1971; Holland, 1972; Burnham, 1979; Cline and Bodnar, 1991; Giggenbach, 1992; Hedenquist and Lowenstern, 1994; Bodnar, 1995).

Though porphyry field relations are well documented, the hydrothermal chemistry of ore elements in these environments is poorly constrained. The situation would be improved if the thermodynamic properties of relevant aqueous complexes were known at magmatic hydrothermal conditions. These data would facilitate quantitative assessment of the relative importance of many physiochemical factors such as, temperature and pressure gradients, ligand availability, pH, redox, phenomena like liquid–vapour immiscibility ('boiling'), and fluid mixing, which affect mineral solubilities, transport, and metal deposition in hydrothermal systems.

High-temperature and -pressure fluids (e.g., >~0.1 GPa, >~350 °C) are, however, difficult to study experimentally owing to their extremely reactive nature. Amongst the more common problems is that fluids quenched from high temperatures may precipitate dissolved material, exsolve or

* Corresponding author. Institute for Mineralogy and Petrology, ETH Zurich, Zurich 8092, Switzerland.
E-mail address: Alistair.Hack@erdw.ethz.ch (A.C. Hack).

0016-7037/$ - see front matter © 2006 Elsevier Inc. All rights reserved.
doi:10.1016/j.gca.2006.04.035

back-react with coexisting phases, such that quenched fluid samples are usually not representative of the experimental conditions (Sourirajan and Kennedy, 1962). This has given rise to various in situ spectroscopic techniques and flow-through systems, but due to the limited physical strength of sample cells/apparatus, investigations have been generally limited to less than a few hundred MPa (e.g., Stefánsson and Seward, 2003; Fulton et al., 2004). Accordingly, specialised experimental techniques have been developed to overcome quench problems and gain access to higher pressure. One established method is to use synthetic inclusions to sample fluids at high pressure and temperature (Bodnar and Sterner, 1987; Bodnar, 1989). The method utilises the fact that hydrothermal re-crystallisation and healing of fluid-filled fractures in minerals is generally imperfect such that samples of the ambient fluid become isolated as inclusions along the annealing fracture and crystal growth surfaces. The advantage of synthetic fluid inclusions is that they remain closed systems on quenching such that the bulk compositional and volumetric properties of the high-temperature fluid are preserved, and hence may be determined using ex situ analytical methods.

Here we present, based on fluid inclusion synthesis experiments, solubility measurements of the assemblage, native copper + cuprite + talc + quartz (Cu + Cpr + Tc + Qz) over a range of Cl concentration, temperature (T) and pressure (P). Fluid compositions were determined from both analysis of synthetic fluid inclusions and quenched fluid samples. The data have been used to investigate copper(I) complexing in supercritical brines and to understand how P, T, and Cl concentration in magmatic-hydrothermal systems affects copper mineral solubility.

1.1. Previous investigations

A number of hydrothermal experimental studies on copper(I)-chloride speciation have been undertaken up to 350 °C, but most are restricted to vapour-saturated pressure (Ahrland and Rawthorne, 1970; Romberger and Barnes, 1970; Crerar and Barnes, 1976; Var'yash and Rekharsky, 1981; Var'yash, 1991; Xiao et al., 1998; Fulton et al., 2000a,b; Liu et al., 2001, 2002; Archibald et al., 2002). Studies by Hemley et al. (1992) and Seyfried and Ding (1993) extend the range of T and P investigated to 500 °C and 0.2 GPa. A current review of these studies is given by Liu and McPhail (2005). Recent determinations of copper(I)-chloride complex stability from solubility and spectroscopic measurements are in general agreement and indicate that mononuclear $CuCl_n^{1-n}$ species dominate under all chloride concentrations investigated (Xiao et al., 1998; Fulton et al., 2000a,b; Liu et al., 2001; Liu et al., 2002). Thermodynamic investigations of copper(I)-chloride complex stabilities have also been made (Helgeson, 1969; Ruaya, 1988; Sverjensky et al., 1997; Akinfiev and Zotov, 2001; Liu and McPhail, 2005). Thermodynamic treatments allow extrapolation of low T data. However, significant changes in H_2O chemistry occur above the critical temperature, and the addition of solutes (e.g., salts, gases, or silicate components) to H_2O results in physically very different conditions at P, T conditions above the critical point of H_2O. Thus, thermodynamic extrapolations above the critical point of H_2O are uncertain in the absence of experimental constraint. The present study considerably extends the experimentally investigated range of pressure, temperature, and salinity, and therefore should be useful in constraining future thermodynamic models.

Other studies have focussed on Cu partitioning between either silicate melt and supercritical aqueous fluid (Ryabchikov et al., 1980; Candela and Holland, 1984; Keppler and Wyllie, 1991) or silicate melt and subcritical brine + -vapor mixtures (Williams et al., 1995). In general, they also show that Cu is strongly coupled to Cl in the fluid, and hence that chlorocopper complexes are important at magmatic conditions (e.g., $CuCl^0_{(aq)}$; Candela and Holland, 1984).

2. Experimental and analytical

2.1. Starting materials

The mineral assemblage talc + quartz + cuprite + native copper was employed to buffer fluid composition. Experimental materials were synthesised from pure chemical reagents (Cu, CuO, $CuCl_2$, and H_2O) and natural minerals (inclusion-free quartz and talc). Talc was characterised by electron microprobe and X-ray diffraction analysis (Table 1). Cu_2O was synthesized at 1 atmosphere in pure Ar at 900 °C for ~24 h from high purity powders of Cu metal and CuO (both >99.9%) mixed in stoichiometric proportions and pressed into pellets. X-ray diffraction analysis confirmed the success of the Cu_2O synthesis. Following standard procedures for fluid inclusion synthesis, crystalline quartz pieces were pre-fractured by heating them to ~350 °C then quenching rapidly in water (Sterner and Bodnar, 1984).

2.2. Fluid inclusion synthesis

Quartz-hosted fluid inclusions were synthesized in pure copper metal capsules containing chloride-bearing H_2O, natural talc, synthetic cuprite, and pre-fractured natural quartz. A 30 mm internal diameter, end-loaded,

Table 1
Talc composition by electron microprobe (wt%)

$N = 19$	$\bar{x}$	σ
SiO_2	60.9	0.8
Al_2O_3	0.06	0.03
MgO	30.4	0.6
FeO	0.50	0.03
Total	91.82	0.78
H_2O	8.18	

piston-cylinder apparatus at the Research School of Earth Sciences, Australian National University (ANU), was used to run the experiments. Piston-cylinder assemblies consisted of a talc + pyrophyllite pressure medium, a graphite furnace sleeve, and a large-volume, cold-sealed capsule (30 mm long and 15 mm OD) to contain the experimental charge. Capsules and lids were machined from a rod of pure Cu metal (>99.9%). Further details of the apparatus, cold-seal capsule, and assembly design, including temperature and pressure calibration data, are given elsewhere (Hack and Mavrogenes, 2006).

Capsules were loaded by weight. Crystalline buffering materials, except for pre-fractured quartz pieces, were ground lightly prior to loading. Typically 0.5 to 0.8 g of distilled, deionised water was added to each capsule. The ratio of the buffering minerals to fluid, excluding the copper capsule, varied between 2.2 and 4.8 (mineral/fluid by mass). The relatively high mineral/fluid ratio reduced the likelihood of any mineral completely dissolving, which would result in an ambiguous experimental result. Additionally, this provides a large surface area for fluid–mineral interactions, promoting rapid equilibration. This is supported by the systematic behaviour of the solubility data and the similarity in the observed compositional uncertainty and that expected from the intrinsic precision of fluid inclusion laser ablation inductively coupled plasma mass spectrometry (LA-ICPMS; ±30 to 50% relative 1σ).

Chlorine was added to the experiments in the form of dried, high-purity $CuCl_2$. It was assumed that the mass of Cl added to a capsule remained constant during the run. After all solids and salt were weighed into the capsule, deionised water was added to give the desired total Cl concentration and approximate fluid density at the conditions of the experiment (the latter was estimated using an equation of state for H_2O, Holland and Powell, 1991). This procedure was found to improve the experimental reliability, as it reduces the volume change (positive or negative) experienced by the cold-sealed capsule between ambient and the applied P, T conditions, thus minimising the likelihood of completely crushing the quartz or fluid leakage.

Piston-cylinder runs were conducted in the following way. First, ~0.2 GPa was applied to the sample prior to heating. Temperature was increased at 50 °C per minute; pressure was increased synchronously, such that the *P–T–time* path approximated a pure water isochore to the desired run P, T. Pressure was adjusted at the final temperature and kept constant for the run duration, by manual adjustment if necessary. Runs were quenched at 50 °C per minute to minimize the thermal shock to the sample. The consequence of using relatively low quench rates was not investigated, but for bulk fluid-inclusion compositions it is unlikely to affect results as isochore-like P–T paths were followed and inclusions remained intact.

2.3. Quench fluid analysis: Mg concentration

After the run, capsules were cleaned, pierced and the residual fluid sampled using a syringe. This solution was weighed and diluted with high-purity, distilled 2% HNO_3 to provide a useful analytical volume and stabilise the dissolved components until analysis, and reweighed. Indium was added as an internal standard to this diluted solution. Quench solutions were analysed for Mg and Cu (and In) by solution inductively coupled atomic emission spectrometry (ICPAES) on a Varian instrument at the Department of Earth and Marine Sciences, ANU. Mg concentrations in the quench solutions were not considered to have changed during quenching. Measured Mg concentrations were used to quantify the fluid inclusion LA-ICPMS data (discussed below, Section 2.4).

Following sampling of the quench solution, capsules were opened and solids were removed for examination. The experiment was considered successful if the complete mineral buffer assemblage was identified in the run products by optical microscopy and, in some cases, by powder X-ray diffraction. Although re-crystallisation and grain size coarsening of the initial buffering minerals was common during the experiments, especially for cuprite (Cu_2O), no new phases were identified in the post-run products. It was not unusual to find large (up to millimetre scale) deep red crystals of cuprite inter-grown with native copper. Quartz crystals were mounted in epoxy and doubly polished for petrographic and LA-ICPMS analysis.

2.4. Fluid inclusion analysis: Cu/Mg and Cu concentrations

Fluid inclusion samples were analysed at the Research School of Earth Sciences, ANU, by excimer ArF ($\lambda = 193$ nm) LA-ICPMS to determine the in situ fluid composition (Günther et al., 1998; Loucks and Mavrogenes, 1999). Specifically, the Cu/Mg concentration ratio was measured for numerous individual fluid inclusions by LA-ICPMS; the average of these measurements was taken as the Cu/Mg concentration ratio of the fluid in the experiment. The absolute Cu concentration was obtained from this ratio using the concentration of Mg in the quench solution sample measured by solution-ICPAES. To check the reliably of this approach, Cu concentrations within individual inclusions from selected runs were measured independently using particle induced X-ray emission (PIXE) at CSIRO, North Ryde, Sydney, following standard procedures (Heinrich et al., 1992). In contrast to the quench solutions, precipitated solutes are preserved within the inclusions and are included in the LA-ICPMS (and PIXE) measurement. Precipitated phases in inclusions were readily identified because they completely dissolved on heating the sample, whereas this was not observed for mineral grains (e.g., cuprite) accidentally trapped in an inclusion at the experimental P, T.

The LA-ICPMS system used employs simple image projection optics with a long working length objective that

gives a large depth of field (~500 μm) such that inclusions well below the surface are still readily ablated. Beam diameter was selected so as to sample the entire inclusion and some of the host mineral, normally 20 to 70 μm. Beam diameter was not varied during ablation. Further details of the instrument design are given elsewhere (Eggins et al., 1998a,b) although the current instrument has been improved by replacement of the previous quadrupole ICPMS with a more sensitive single collector Agilent 7500 series quadrupole ICPMS. Time-resolved data were collected at one point per mass peak with dwell time per mass set at 10–20 ms and with counting carried out in dual detector (pulse and analogue) mode. Laser ablation frequency (15–25 Hz), sample carrier gas (He–Ar) flow and plasma conditions were tuned for optimum sensitivity, i.e., counts/μg/g, on analyte masses and subject to ThO/Th < 0.5%, for each analytical session. Synthetic soda-lime aluminosilicate glasses NIST SRM 610 and 612 were used for calibration (NBS, 1970; Pearce et al., 1997). Appropriate corrections for instrument drift, depth dependent signal attenuation, and host signal contribution were applied to the raw LA-ICPMS data.

3. Results

3.1. Fluid inclusion petrography

At ~25 °C fluid inclusions from most individual experiments consisted of a vapour bubble, liquid and a distinctive colourless to brown, tetrahedral daughter crystal, identified as nantokite, CuCl (Fig. 1). The distinctive tetrahedral daughter crystal is observed in all of the Cl-bearing experiments but not in Cl-free fluid inclusions (Fig. 2). Various attempts to identify the precipitated mineral (nantokite) using PIXE and Raman spectroscopy were unsuccessful because it invariably decomposed under the incident beam. However, XANES spectroscopic data were acquired confirming it as nantokite (Berry et al., 2006). It is worth noting that the appearance of nantokite is similar to triangular opaque daughter minerals found in many natural inclusions that are usually identified as chalcopyrite, but that chalcopyrite does not decompose under the incident beam (our experiments do not contain sulfur or iron, so the daughter mineral observed here can not be chalcopyrite).

Phase proportions are uniform for individual experiments and vary systematically with the synthesis P–T–X conditions, i.e., the relative volume of vapour bubbles in inclusions increased with increasing T, at constant P and constant salinity, consistent with the decrease in fluid density. Similarly, the relative volume of daughter nantokite increased with increasing Cl concentration, at constant T and P, consistent with higher Cu concentrations at higher chloride. Inclusions completely homogenised on heating; daughter nantokite always dissolves at a T well below the T of formation, hence fluids were not saturated with this mineral at the inclusion trapping conditions. The observed characteristics were interpreted as being consistent with equilibrium (with Cu + Cpr + Tc + Qz) at the run conditions.

The fluid density of inclusions formed above ~1.5 GPa at 710 °C is sufficiently high that no bubble nucleates on

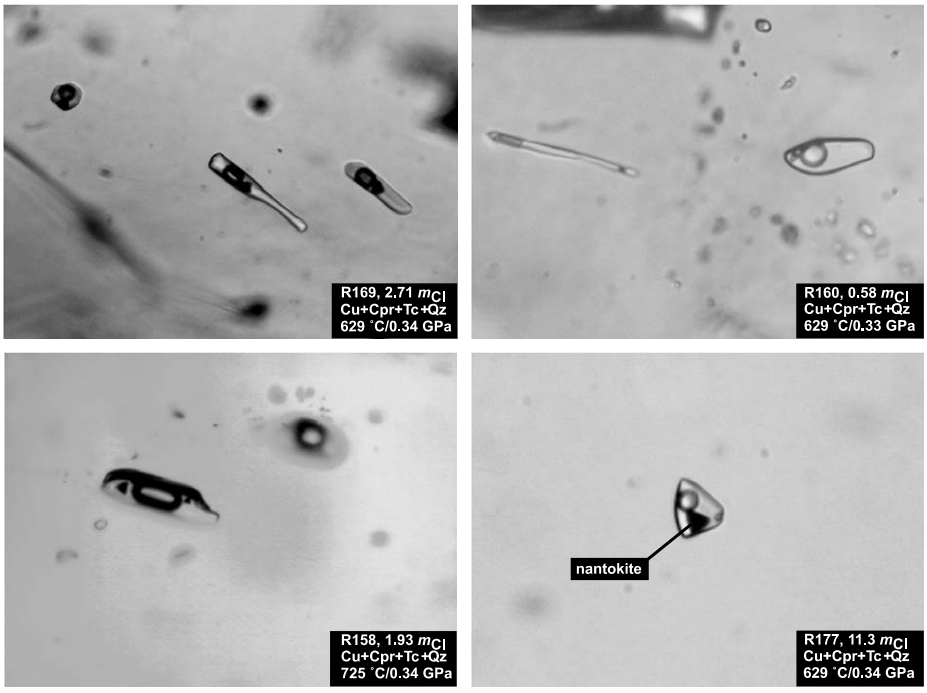

Fig. 1. Photomicrographs at 25 °C of typical quartz-hosted aqueous fluid inclusions synthesised at various P–T–X conditions. All inclusions contain nantokite as a daughter mineral. Inclusions in these images are approximately 20–50 μm.

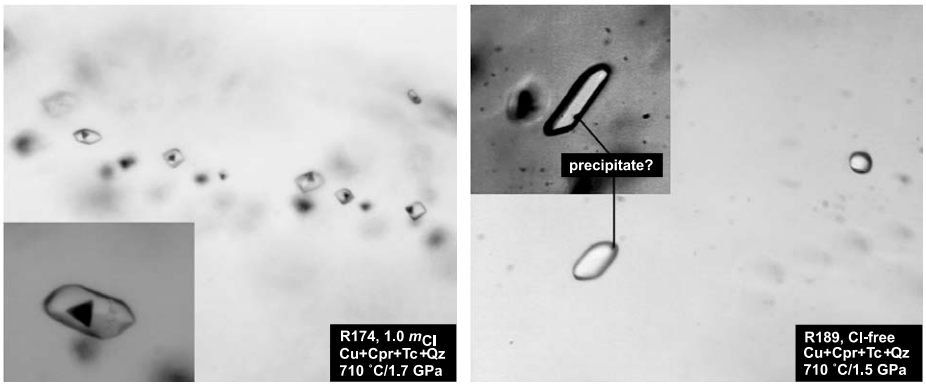

Fig. 2. Photomicrographs at 25 °C of quartz-hosted high-density fluid inclusions synthesised at 710 °C, 1.7 GPa (R174) and 1.5 GPa (R189) in 1 mol kg^{-1} Cl and Cl-free aqueous fluid, respectively, and buffered by Cu + Cpr + Tc + Qz. Daughter mineral in Cl-bearing inclusions is nantokite, Cl-free fluid inclusions may contain some other quench precipitated phase but it was too small to identify. Inclusions in these images are 10–35 μm. Insets: enlarged view of typical fluid inclusions.

cooling (Fig. 2). Such high-density fluid inclusions are internally over-pressured at room conditions. Accordingly, intact natural inclusions from similar P, T are rare as they usually decrepitate during decompression (Invernizzi et al., 1998).

3.2. Quenched fluids

Fresh quench solutions were initially colourless and often cloudy. The absence of Cu^{2+} at high T was confirmed by XANES microspectroscopy on individual homogenised fluid inclusions from this study (Berry et al., 2006). The small amounts of capsule solution that could not be extracted turned greenish-blue after exposure to air. This was interpreted as oxidation of the dissolved copper. Cloudiness of the solutions was attributed to precipitation of dissolved silica and nantokite on quenching.

Invariably, capsule solution compositions (as opposed to bulk inclusion compositions) were partially modified on quenching. This was indicated by lower Cu/Mg concentration ratios for the quenched solution than for fluid inclusions (measured by LA-ICPMS) from the same run. Petrographic examination of the synthetic fluid inclusions indicates the discrepancy is due to Cu loss on cooling, as quench modified elements, i.e., Cu and Cl were identifiable in daughter nantokite in inclusions at room temperature. Similarly, individual fluid inclusion analyses using PIXE indicate higher Cu concentrations than is consistent with quench solution measurements. In contrast, there is no evidence that Mg concentration was affected on quenching, as no Mg-bearing daughter phases were observed in fluid inclusions at room temperature or in the quenched run products taken from the capsule. Another compelling reason for not suspecting modification of Mg concentrations in quench solutions is that analysed Mg concentrations vary systematically with the run conditions (i.e., P, T, and Cl concentration) and were at the parts per million (ppm) level, well below the concentration required to precipitate magnesium chloride (i.e., 35.2 wt% $MgCl_2$ at 20 °C). Thus, although we cannot be completely certain, we consider it unlikely that Mg changed during quenching.

3.3. Fluid compositions

Experimental details and dissolved element concentrations in equilibrium with Cu + Cpr + Tc + Qz are reported in Table 2 and plotted in Fig. 3. Solid lines on Fig. 3 show the results of a least squares fit to all of the measurements (Table 3). Dashed lines on Fig. 3 indicate the upper and lower 95% confidence bounds on the least square fit and indicate the regions which are least well constrained by the measurements. Part of the mismatch apparent between experimental data and smoothed fit is related to deviations in the experimental conditions from the conditions at which the calculation was made (cf. Table 2).

As evident in Fig. 3, total dissolved Cu concentrations are always 1 to 2 log units (molal) higher than total dissolved Mg at all conditions. In the present fluids Cu and Cl are major solutes (both >1 wt%) whereas Mg occurs as a trace solute (~100 to 1000 ppm). Consequently $[Cl]_t/[Cu]_t$ gives a first order approximation of the average stoichiometry of the copper(I) complexes present. Figs. 3a and c show that both total dissolved Mg and Cu concentrations increase with increasing total Cl and also increase with increasing P. The pressure series data indicate that fluids above ~0.5 GPa (710 °C) have a molar $[Cl]_t/[Cu]_t < 1$ (Fig. 3c), whereas for the salinity series $[Cl]_t/[Cu]_t$ varies from 1 up to 4 at the highest salinities investigated (11.3 mol kg^{-1} Cl). Fig. 3b shows that with increasing T from 524 to 725 °C both total dissolved Cu and Mg concentrations decrease, approximately fourfold and twentyfold respectively. Also with increasing T the fluid $[Cl]_t/[Cu]_t$ varies from 0.9 up to 2.4. As will be shown, these variations can be attributed to changes in

Table 2
Experimental details and dissolved element concentration measurements for Cu + Cpr + Tc + Qz buffered fluids

	T/°C	P/GPa	Time	mineral/fluid	$[Cl]_t$/mol kg^{-1}	$[Cu]_t$/mol kg^{-1}	N (flinc)	$[Mg]_t$/mol kg^{-1}
Salinity series								
R159	629	0.330 ± 0.006	289	2.4	0.285	0.21 ± 0.05	22	0.0059 ± 0.0001
R160	629	0.330 ± 0.003	265	2.9	0.576	0.59 ± 0.14	12	0.0081 ± 0.0006
R161	629	0.334 ± 0.003	355	2.8	0.876	0.74 ± 0.13	12	0.008526 ± 0.000078
R162	629	0.370 ± 0.006	353	3.5	1.175	0.92 ± 0.18	36	0.0176 ± 0.01
R163	629	0.334 ± 0.003	380	4.7	1.485	1.06 ± 0.34	16	0.0223 ± 0.0013
R164	629	0.331 ± 0.006	307	4.5	2.132	2.63 ± 0.49	4	0.02963 ± 0.00082
R169	629	0.341 ± 0.001	264	3.1	2.705	0.84 ± 0.36	70	0.02479 ± 0.00092
						1.6 ± 0.47	*4*	
R173	629	0.334 ± 0.003	141	2.6	3.826	3.19 ± 0.54	15	0.04 ± 0.00083
R178	629	0.334 ± 0.003	162	3.4	5.666	1.35 ± 0.17	13	0.02831 ± 0.00039
R176	629	0.364 ± 0.005	137	3.2	7.323	2.33 ± 0.45	44	0.035 ± 0.018
R177	629	0.338 ± 0.006	171	4.4	11.283	3.95 ± 0.47	48	0.064 ± 0.0098
Temperature series								
R153	524	0.334 ± 0.003	454	3.2	2.117	1.45 ± 0.19	43	0.084 ± 0.00079
R156	599	0.390 ± 0.007	336	4.0	1.929	1.83 ± 0.65	13	0.030 ± 0.011
R164	629	0.331 ± 0.006	307	4.5	2.132	*2.45 ± 0.5*	*4*	0.0296 ± 0.0056
R157	650	0.334 ± 0.003	263	3.0	1.926	1.01 ± 0.24	12	0.0224 ± 0.0025
R158	725	0.335 ± 0.006	188	3.3	1.926	0.38 ± 0.09	19	0.00439 ± 0.00064
Pressure series								
R183	710	0.313 ± 0.014	138	2.2	1.00	0.92 ± 0.14	54	0.0062 ± 0.0023
R171	710	0.662 ± 0.005	235	2.4	1.00	1.31 ± 0.34	13	0.0178 ± 0.00052
						1.5 ± 1.0	*7*	
R172	710	0.991 ± 0.003	168	2.2	1.00	2.27 ± 0.76	8	0.147 ± 0.058
R174	710	1.703 ± 0.007	158	3.1	1.00	3.78 ± 0.62	49	0.213 ± 0.012
R189	710	1.494 ± 0.012	146	4.8	0.00	0.075 ± 0.009	24	0.006 ± —

Notes. Run duration is in hours. Mineral/fluid is the mass ratio of buffering minerals to H_2O (capsule and initial salt mass are not included in this ratio). $[Cl]_t$ is the total Cl concentration measured at start of experiment. $[Cu]_t$ is the mean Cu concentration obtained from N individual fluid inclusion (flinc) measurements by LA-ICPMS; PIXE fluid inclusion measurements are italicised. $[Mg]_t$ is the total Mg concentration obtained by solution-ICPAES analysis of quenched solution sampled from capsule after the experiment. Concentration uncertainties are 95% confidence limits about the mean.

the speciation of the dissolved elements as a function of $[Cl]_t$, T, and P.

4. Data interpretation

Our aim is to identify the average stoichiometry of copper(I) complexes present at a given condition. Thermodynamic data can be obtained from solubility measurements of an assemblage which defines the chemical potentials of all components in the system (Crerar et al., 1978; Barnes, 1981). Applying Gibbs' phase rule, our system of interest contains six components (Cu–Cu_2O–MgO–SiO_2–HCl–H_2O) and five phases (Cu + Cpr + Tc + Qz + fluid), leaving three degrees of freedom, which were eliminated by fixing P, T, and total Cl in each experiment. Thus, we have attempted to interpret the solubility data using a thermodynamic model that includes the aqueous species likely to be significant at the experimental conditions and the relevant mass action, mass balance, charge balance and activity coefficient equations. Due to the limited number of data and to account for minor variations in P or T or $[Cl]_t$ within each experimental series the solubility model was fit directly to the least square fit (Table 3). Fig. 3 indicates the uncertainty associated with the fit to the data.

4.1. Solubility model

The solubility of Cu + Cpr + Tc + Qz can be represented by the following equilibria,

$$1/2Cu_2O_{(Cuprite)} + H^+_{(aq)} = Cu^+_{(aq)} + 1/2H_2O_{(liq)} \quad (1)$$

$$1/2Cu_2O_{(Cuprite)} + nHCl^0_{(aq)} = CuCl(HCl)^0_{n-1(aq)} + 1/2H_2O_{(liq)} \quad (2)$$

$$Cu_2O_{(Cuprite)} + H^+_{(aq)} = Cu_{(Native)} + CuOH^0_{(aq)} \quad (3)$$

$$1/3Mg_3Si_4O_{10}(OH)_{2(Talc)} + 2\ H^+_{(aq)} = 4/3SiO_{2(Quartz)} + Mg^{2+}_{(aq)} + 4/3\ H_2O_{(liq)} \quad (4)$$

$$SiO_{2(Quartz)} = SiO^0_{2(aq)} \quad (5)$$

$$H^+_{(aq)} + Cl^-_{(aq)} = HCl^0_{(aq)} \quad (6)$$

$$Mg^{2+}_{(aq)} + Cl^-_{(aq)} = MgCl^+_{(aq)} \quad (7)$$

$$MgCl^+_{(aq)} + Cl^-_{(aq)} = MgCl^0_{2(aq)} \quad (8)$$

$$Mg^{2+}_{(aq)} + OH^-_{(aq)} = MgOH^+_{(aq)} \quad (9)$$

$$H^+_{(aq)} + OH^-_{(aq)} = H_2O_{(liq)} \quad (10)$$

mass balance equations,

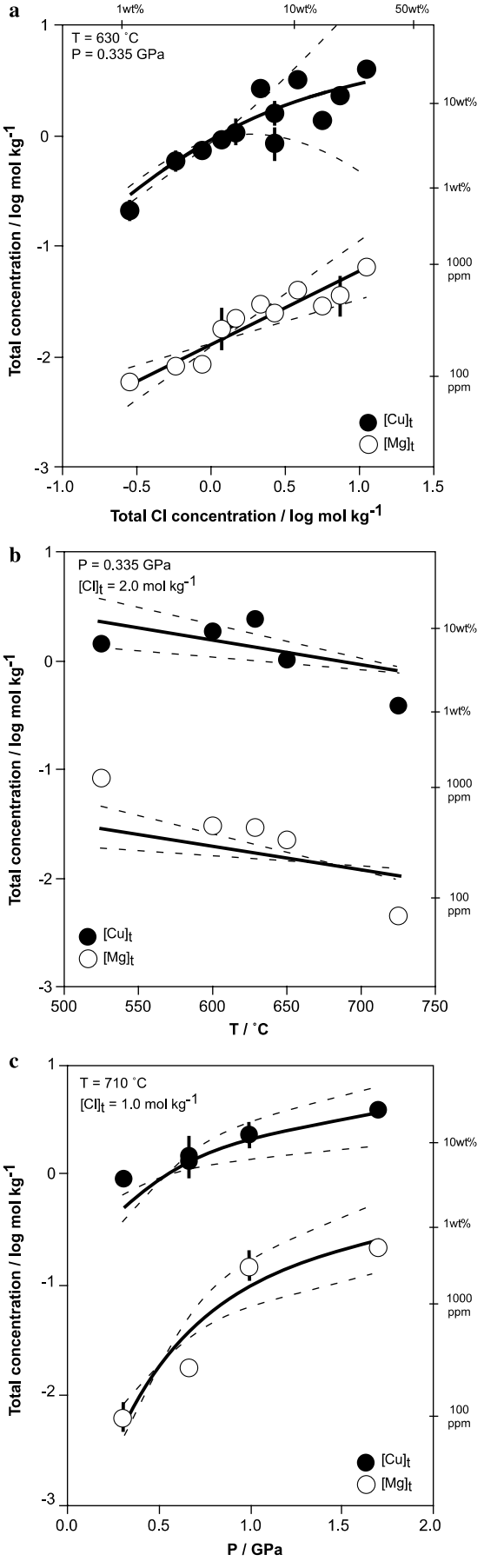

Fig. 3. Experimental dissolved Cu (filled circle) and Mg (open circle) concentrations in fluids buffered by the mineral assemblage Cu + Cpr + Tc + Qz for: (a) salinity series; (b) temperature series; and, (c) pressure series. Measurement uncertainty (±95% confidence) indicated where larger than the symbol; concentration by mass (ppm, wt%) shown on alternate axes. Solid lines are calculated from the least squares fit for the conditions indicated, dashed lines are the upper and lower 95% confidence bounds on the fit (Table 3).

$$[\mathrm{Cl}]_t = n \cdot [\mathrm{CuCl(HCl)}^0_{n-1(aq)}] + [\ \mathrm{HCl}^0_{(aq)}] + [\mathrm{Cl}^-] + 2[\mathrm{MgCl}^0_{2(aq)}] + [\ \mathrm{MgCl}^+] \quad (11)$$

$$[\mathrm{Cu}]_t = [\mathrm{Cu}^+] + [\mathrm{CuCl(HCl)}^0_{n-1(aq)}] + [\ \mathrm{CuOH}^0_{(aq)}] \quad (12)$$

$$[\mathrm{Mg}]_t = [\mathrm{MgCl}^0_{2(aq)}] + [\mathrm{MgCl}^+] + [\ \mathrm{MgOH}^+] + [\mathrm{Mg}^{2+}] \quad (13)$$

$$[\mathrm{SiO_2}]_t = [\mathrm{SiO}^0_{2(aq)}] \quad (14)$$

$$X_{\mathrm{H_2O}} = 1 - \sum_{i=1}^{N} X_i \quad (15)$$

where X_i is the mole fraction of the ith species and the sum includes and the sum includes all, N, species; and, charge balance equation,

$$0 = [\mathrm{Cu}]^+ + [\mathrm{MgCl}^+] + [\mathrm{MgOH}^+] + 2[\ \mathrm{Mg}^{2+}] + [\mathrm{H}^+] - [\mathrm{OH}^-] - [\mathrm{Cl}^-] \quad (16)$$

where, $[j]_t$ is the total dissolved molal concentration of j, and $[i]$ is the molal concentration of the ith species. The coefficient n (equilibrium 2) describes the average stoichiometry of copper(I)-chloride species present.

Several preliminary speciation models were tested for their ability to reproduce the least squares to fit to the entire experimental data set. We found that our initial speciation models containing conventional CuCl_n^{1-n}-type complexes were unable yield a solution matching that of the smoothed data where $[\mathrm{Cl}]_t/[\mathrm{Cu}]_t > \sim 1$. This problem was not encountered when neutral chlorocopper(I) complexes with the general formula $\mathrm{CuCl(HCl)}^0_{n-1(aq)}$ were considered (equilibrium 2). We also found that it was not possible to fit the data above 0.5 GPa where the solutions have molar $[\mathrm{Cl}]_t/[\mathrm{Cu}]_t < 1$, without including hydroxide complexing (equilibrium 3).

Equilibria (1–3) indicate that cuprite solubility is sensitive to changes in acidity (pH) and the activity of $\mathrm{HCl}^0_{(aq)}$. The coexistence of talc and quartz controls acidity by fixing the $a_{\mathrm{Mg^{2+}}}/(a_{\mathrm{H^+}})^2$ ratio of the fluid (equilibrium 4). At constant P and T, pH and $a_{\mathrm{HCl}^0_{(aq)}}$ are fixed according to the amount $[\mathrm{Cl}]_t$ in the experimental solution. The coexistence of native copper and cuprite buffers the redox potential of the system, via $2\mathrm{Cu} + \mathrm{H_2O} = \mathrm{Cu_2O} + \mathrm{H_2}$, such that copper(I) is the oxidation state in the experimental solutions, and has been confirmed by XANES spectroscopy on homogenised fluid inclusions (Berry et al., 2006).

4.1.1. Standard state and activity coefficient conventions

Equilibrium constants (k) are defined in the usual way for reactions (1), (4–10) as the product $k = \prod_i a_i^{v_i}$, where a

Table 3
Least square fit to the experimental data

	$[Cu]_t$	$[Mg]_t$
a_0	418 ± 101	-776 ± 120
a_1	3.5 ± 0.8	6.9 ± 0.9
a_2	0.75 ± 0.16	0.68 ± 0.13
a_3	-0.24 ± 0.21	—

$\log[j]_t = a_0 T^{-1} + a_1 \log \rho H_2O + a_2 \log[Cl]_t + a_3 (\log[Cl]_t)^2$.
Notes. $[j]_t$ and $[Cl]_t$ in mol kg^{-1}, T in K, ρH_2O is the density of pure H_2O at the P, T of interest (Holland and Powell, 1991), and a_m are the fitted parameters.

is the thermodynamic activity, which for the ith aqueous species is $a_i = \gamma_i \cdot m_i$, and γ and m refer to the activity coefficient and molal concentration, respectively, v_i is the stoichiometric coefficient and is positive for products and negative for reactants. The standard state used for aqueous species was the conventional, hypothetical ideal one molal solution referenced to infinite dilution at the P, T of interest. The standard states for solid phases and H_2O were defined as the pure mineral and liquid at the P, T of interest. Since essentially pure minerals were employed their activities were taken as unity. The activity of H_2O was assumed equal to its mole fraction (Eq. (15)). A modified Davies formulation of the Debye–Hückel equation was used to calculate the molal activity coefficients of individual charged species ($\gamma_i^{+/-}$),

$$\log \gamma_i^{+/-} = -\frac{A_\gamma z_i^2 \bar{I}^{0.5}}{1 + \bar{I}^{0.5}} + 0.2 A_\gamma z_i^2 \bar{I}, \quad (17)$$

where the subscript i, refers to the ith species, A_γ is a species-independent Debye–Hückel solvent parameter. There are no experimental data that allow calculation of A_γ over the range of P and T in the present study. Accordingly, we use the approximation $A_\gamma = 1.0\ kg^{1/2}\ mol^{1/2}$ in all calculations. This assumption follows Manning (1998), who noted that: (a) although A_γ changes depending on P and T, at pressures above ~0.4 GPa it approaches a narrow range of constant values near unity (e.g., $1.0 \pm \sim 0.3\ kg^{1/2}\ mol^{1/2}$); and, (b) that, speciation calculations are relatively insensitive to the use of different A_γ values within this range. z_i is the valence of the ith species. $\bar{I}$ is the ionic strength of the solution,

$$\bar{I} = \frac{1}{2} \sum_{i=1}^{N} z_i^2 [i]. \quad (18)$$

Most Debye–Hückel type equations become inaccurate at ionic strengths greater than $\sim 1.0\ mol\ kg^{-1}$, but activity models more complex than that represented by the Davies Eq. (17) contain additional parameters which are unconstrained over the conditions investigated. Thus, for our purposes we consider the simplicity of the Davies equation to offset its potential limitations.

Activity coefficients of neutral species were assigned a value of one on the basis that this is the simplest assumption in light of the uncertainty associated with the behaviour of activity coefficients for such species (cf. Walther, 1997; Oelkers and Helgeson, 1991).

4.1.2. Thermodynamic data for Cu^+ and $MgO–SiO_2–H_2O–HCl$ subsystem and extrapolation of equilibrium constants to high pressure

To derive details about the general stoichiometry of the dissolved Cu^+ complexes the solubility model requires log k values for the subset of mineral-fluid equilibria in the $MgO–SiO_2–H_2O–HCl$ system (equilibria 4–10) and equilibrium (1). Appendix A lists the equilibrium constant values and thermodynamic data sources used in all regression model calculations. Since the thermodynamic properties of most aqueous species are experimentally unconstrained at pressures above a few hundred MPa and few theoretical models allow for extrapolation to pressures above ~0.5 GPa (e.g., the HKF model is limited to $P \leqslant 0.5$ GPa, Helgeson et al., 1981), the empirical approach of Manning (1998) was employed to estimate log k values up to 1.7 GPa. Manning (1998) noted that at constant T, log k's for many aqueous equilibria vary as a linear

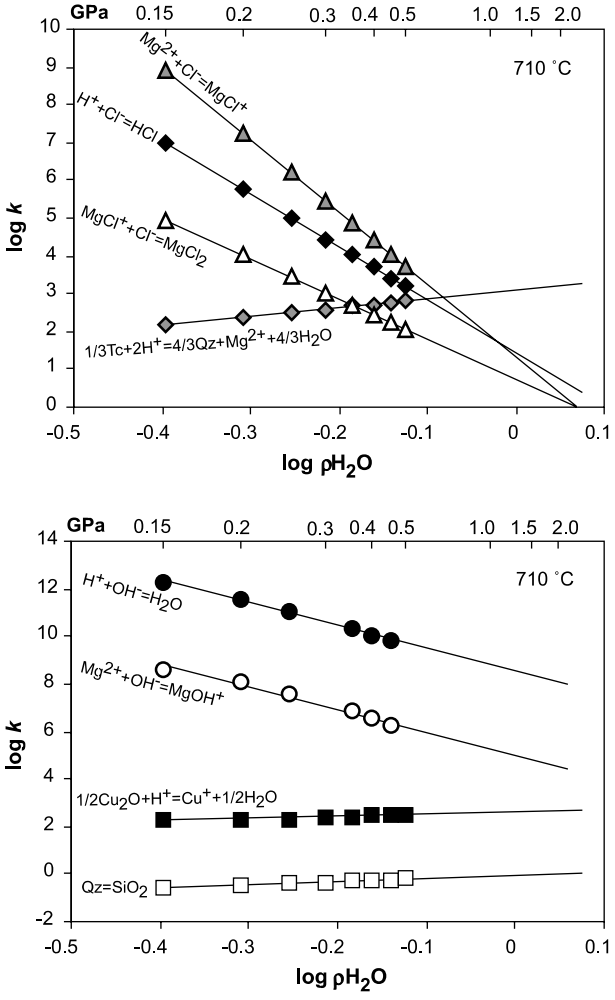

Fig. 4. Log k versus log ρH_2O at 710 °C. Symbols represent log k values calculated from the literature for the indicated equilibrium. Solid lines represent linear least square fits to the calculated data ($P \leqslant 0.5$ GPa) and were used to obtain log k estimates to 1.7 GPa for solubility model calculations. Pressure corresponding to log ρH_2O at 710 °C is given on the upper abscissa.

function of log H_2O density (log ρH_2O) and showed that this relation can be used to obtain an approximation of log k to at least 2.0 GPa. The computer program Supcrt (Johnson et al., 1992) was used to calculate log k values at the T of interest from 0.15 to 0.5 GPa. These values were plotted against log ρH_2O (Holland and Powell, 1991) and a linear least squares fit equation was used to estimate log k above 0.5 GPa. Fig. 4 illustrates the extrapolation results.

4.1.3. Speciation calculations

A non-linear Generalised Reduced Gradient algorithm was used to iteratively vary the concentration of each species and n so as to minimise the difference between the empirical least square fit to the experimental dataset and the calculated mineral solubility as defined by a simultaneous solution of Eqs. (1)–(18) and the constraint $n \geqslant 1$. As $[Cl]_t$ was not varied at all P, T conditions investigated, no attempt was made to derive individual copper(I) complex formation constants. Instead we use the solubility model to find the concentration of copper(I)-chloride complexes and their average Cl coordination number (n), or where $n = 1$, $CuOH^0$ was included in the copper(I) speciation also. In this model only two unknowns were solved for at any given P–T–X. Numerical upper and lower bounds were imposed on all variables to restrict them to physically meaningful values during the iterations, calculations were performed using the 'solver' function in the Microsoft Excel software.

5. Discussion

5.1. Solubility model results: copper(I) speciation

Copper(I) speciation results (n and distribution of chloride- and hydroxide-complexes) from the solubility modelling are plotted in Fig. 5 as a function of $[Cl]_t$, T, and P. These results show copper(I) speciation is predominated by $CuCl(HCl)^0_{n-1}$ over the entire range of conditions covered by the salinity and temperature series data, i.e., $n \geqslant 1$ (Figs. 5a and b). Minor $CuOH^0_{(aq)}$ (2.5% of total Cu species) was detected at the lowest salinity considered (0.285 mCl), and is preliminary evidence that copper(I)-hydroxide species become important at lower salinities (Fig. 5a). Variations in total Cu concentration with increasing salinity at constant P, T (Fig. 3a) and increasing T at constant P and $[Cl]_t$ (Fig. 3b) are explained by increasing average chloride coordination number, n, of $CuCl(HCl)^0_{n-1}$ complexes from 1 to ~4 and 1 to ~2.5 respectively (Figs. 5a and b). However, note that for most salinities and temperatures $n \leqslant 2$ occurs, and seems, at least circumstantially, consistent with previous investigations (e.g., Candela and Holland, 1984). Although it was not investigated in the temperature or pressure series, we expect the coordination of copper(I)-chloride complexes at $T >$ ~650 °C, $P > 0.3$ GPa to also be sensitive to changes in $[Cl]_t$.

The observed increase in n with increasing T is consistent with the notion that ion association and complex

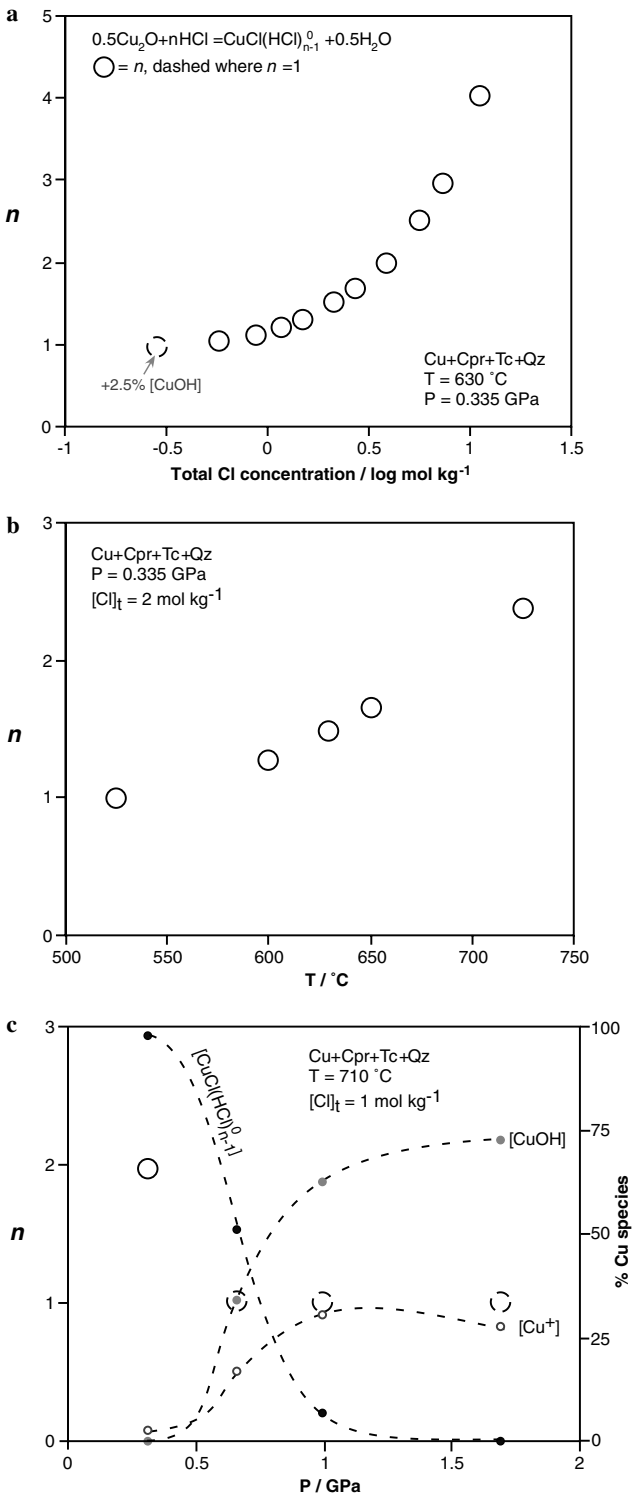

Fig. 5. Results of solubility model fit to the smoothed experimental data. Open circles indicate average ligand number (n) of $CuCl(HCl)^0_{n-1}$ complexes in aqueous fluid in equilibrium with Cu + Cpr + Tc + Qz (broken open circles indicate where $n = 1$). (a) log total Cl (mol kg^{-1}), for $T = 630$ °C, $P = 0.335$ GPa (for $\log[Cl]_t = -0.55$, $n = 1$ and 2.5% $CuOH^0_{(aq)}$ occurs in the speciation calculation); (b) temperature, for $P = 0.335$ GPa, $[Cl]_t = 2$ mol kg^{-1}; and, (c) pressure, for $T = 710$ °C, $[Cl]_t = 1$ mol kg^{-1}, labelled dashed curves show the copper(I) species distribution (note, at 1.7 GPa the model calculation did not converge on a satisfactory solution for $[Mg]_t$, a solution was found at all other conditions).

formation are generally favoured by increasing T at constant P (Oelkers and Helgeson, 1990). That is, higher-order molecular complexes are stabilised at higher temperatures. This may seem counterintuitive but the formation of complexes is usually thought to result in an entropy gain related to a decrease in the total coordination number of the associated species due to the liberation of H_2O molecules from hydration shells (Helgeson, 1964).

In contrast to the salinity and temperature series, modelling results for the pressure series indicate that the increase in Cu solubility with increasing P is due to the predominance of $CuOH^0_{(aq)}$ over copper(I)-chloride complexes for $P \geqslant 0.5$ GPa (Fig. 5c). The relation between P, T and stability of individual complexes is not well constrained by the current data, preventing a more detailed treatment.

5.2. Calculations using existing thermodynamic data for copper(I) complexes

Although we have already made the point that we were unable to explain the present data using existing or conventional speciation schemes, the present experimental data nonetheless provide an opportunity to examine the accuracy of existing thermodynamic models to predict mineral solubilities outside the range of conditions at which they were initially obtained. Two recent studies (Akinfiev and Zotov, 2001; Liu and McPhail, 2005) report thermodynamic properties for various aqueous copper(I)-chloride and -hydroxide species in the form of revised Helgeson–Kirkham–Flowers (HKF) equation of state parameters (Tanger and Helgeson, 1988) allowing them to be easily compared and extrapolated to high T and P. The formation constants for copper(I)-chloride complexes, predicted by Liu and McPhail (2005) and Akinfiev and Zotov (2001) at elevated T and P are in significant disagreement, e.g., predicted formation constant for $CuCl_2^-$ differs by 2.8 log units at 725 °C, 0.335 GPa (Appendix B). The reason for the discrepancy is unclear, though we note more data was available to Liu and McPhail (2005). Accordingly, we made two model solubility calculations, one using properties reported by Liu and McPhail (2005)) for copper(I)-chloride complexes, and the other using data reported by Akinfiev and Zotov (2001) for both copper(I)-chloride and copper(I)-hydroxide complexes. For these calculations, saturation with Tc + Qz + Cu + Cpr was assumed and only P, T, and $[Cl]_t$ were specified, such that $[Cu]_t$ and $[Mg]_t$ were calculated entirely from log k values for mineral-fluid equilibria (Appendices A and B) in the alternate copper(I) speciation models and appropriately modified mass and charge balance, and activity-composition constraints (Eqs. (11)–(18)). Fig. 6 shows the measured solubilities from the salinity, temperature and pressure series and those predicted using existing alternate sources of thermodynamic data for aqueous Cu^+ speciation. The P, T, and $[Cl]_t$ conditions at which the model calculations were made are given on the figures.

Fig. 6 shows that calculated total dissolved element concentrations differ significantly depending on whether Cu^+ speciation is based on the data of Liu and McPhail (2005) or Akinfiev and Zotov (2001), and yet neither model accurately predicts the measured trends for *both* Mg and Cu. Such discrepancies are probably not surprising given that mineral solubility calculations require a number of assumptions, not least that the underlying thermodynamic framework correctly describes the system, e.g., the revised HKF model equations, data taken for all species and activity-composition models chosen are appropriate, and importantly that the species considered are those stable at the conditions of interest. These potential criticisms also apply equally to our model-dependent interpretation of the solubility data. The point we wish to make is, for existing speciation schemes to reproduce the measurements, changes to the thermodynamic model are necessary, alternatively we suggest the present data may also be plausibly explained by the formation of complexes not observed at lower P, T.

5.3. Evidence from X-ray absorption near-edge structure (XANES) spectroscopy

The literature provides little theoretical guidance as to whether complex formation or modification of existing thermodynamic models, e.g., to use activity coefficients to describe non-ideal interactions between solvated $CuCl^0$ and HCl^0 molecules, is the most appropriate way to interpret our solubility data. To help resolve the issue a limited selection of samples were investigated using XANES spectroscopy (details will be reported elsewhere by Berry et al. (2006)). XANES is an element specific technique which can yield information on the oxidation state and coordination environment. To obtain information on in situ speciation, Cu *K*-edge XANES spectra were collected for homogenised fluid inclusions. XANES spectra for high salinity fluid inclusions (R177, $[Cl]_t = 11.3$ mol kg^{-1}) indicate the presence of highly coordinated Cu^+ species, i.e., $CuCl(HCl)^0_{3(aq)}$ in, whereas in lower salinity fluid inclusions (R169, $[Cl]_t = 2.7$ mol kg^{-1}) Cu^+ is in linear coordination with one or two Cl, as $CuCl^0_{(aq)}$ or $CuCl(HCl)^0_{(aq)}$. The XANES data provide no information on the ionisation state of the complex(es), a neutral configuration is indicated by our solubility model. Although the XANES data are not sufficiently extensive to quantify the species distribution the results are in broad agreement with our interpretation of the solubility data.

5.4. Copper concentrations in magmatic fluids

The concentration of Cu in many magmatic-hydrothermal fluids is thought to be significant (>~1 wt%) as chalcopyrite daughter crystals have been observed in high-salinity aqueous liquid inclusions at several localities: Sar Cheshmeh, Iran (Etminan, 1977); Panguna, Bougainville, Papua New Guinea (Eastoe, 1978); Red

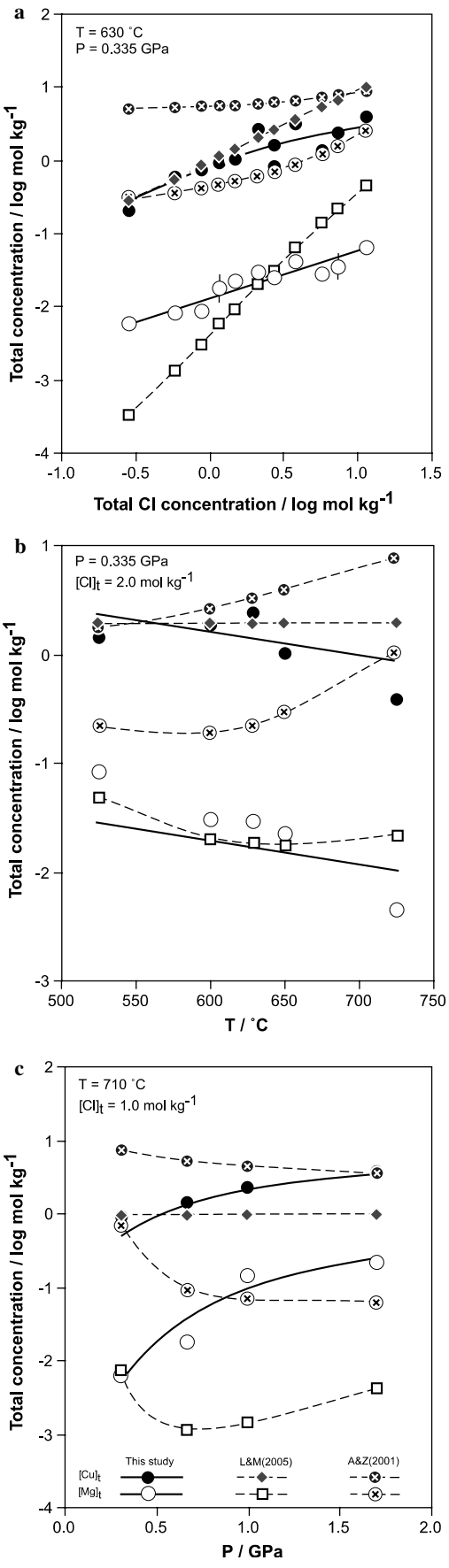

Fig. 6. Comparison of different model calculations made using existing thermodynamic data and the total dissolved element concentration data corresponding to: (a) salinity series; (b) temperature series; and, (c) pressure series data.

Mountain, Arizona (Bodnar and Beane, 1980); Sonora district (breccia pipes), Mexico (Sawkins and Scherkenbach, 1981); Santa Rita, New Mexico (Reynolds and Beane, 1985); Big Gossan, Ertsberg, Irian Jaya (Meinert et al., 1997); and Bajo de la Alumbrera, Argentina (Ulrich et al., 1999; Harris et al., 2003). Recently, quantitative fluid inclusion measurements have shown Cu is present up to a few weight percent, and at some localities preferentially partitions into the vapour (Heinrich et al., 1992; Heinrich et al., 1999; Ulrich et al., 1999, 2001). It is notable, however, that the inclusion study by Harris et al. (2003) reports that the most primitive fluids at Bajo de la Alumbrera are brines containing ~15 wt% Cu. Thermodynamic mineral solubility calculations, based on extrapolation of low T experimental data, also indicate weight percent Cu concentrations should be typical of high T (i.e., >~450 °C) porphyry copper environments (e.g., Hezarkhani et al., 1999; Liu and McPhail, 2005).

Not surprisingly there pervades a well-founded general view that at high T, Cu concentrations can be extremely high (>~1 wt%). The present experimental measurements (up to ~15 wt% Cu) are significant because they give additional credence to the interpretation of many natural samples - that dissolved Cu concentrations can be very high and easily adequate, i.e., Cu ⩾ 1000 ppm (Rose, 1970), for forming a typical porphyry copper deposit. It also seems likely that, in the absence of other evidence, natural inclusions containing higher Cu concentrations than found here are not fluid-only compositions but result from co-entrapment of a Cu-rich phase (e.g., sulfide melt/mineral) and fluid during the inclusion formation.

The absence of ores precipitated at near-magmatic temperatures (i.e., ~500 to 850 °C) is probably related to the high solubility of Cu at these conditions, such that initial dissolved Cu concentrations in fluids exsolved from most magmas are always far from saturation, even at concentrations of a few weight percent.

5.5. Ore deposition and transport processes in porphyry systems

Field relations constrain hydrothermal ore deposition and transport processes in porphyry environments. There is a conspicuous absence of Cu ore deposition above ~450 °C, despite considerable evidence suggesting the primary ore fluids have a magmatic origin. Three general processes are thought important in ore deposition from porphyry hydrothermal fluids: (1) fluid mixing; (2) cooling; and, (3) fluid decompression and 'boiling' (Crerar and Barnes, 1976; Brimhall and Crerar, 1987; Hezarkhani et al., 1999). We consider these processes, tentatively

assuming that the general results found here are also likely to be observed for Cu in other mineral-buffered systems.

5.5.1. Fluid mixing: ore deposition or dissolution?

It is widely recognised that Cu mineral solubility is influenced by Cl concentration in aqueous hydrothermal fluids. Similarly, it is broadly understood that exsolved magmatic fluids which are thought to be the principle source of metals and gases inevitably interact and disperse within ambient dilute convecting groundwaters (Henley and McNabb, 1978; Heinrich et al., 2004). Numerous workers have proposed that the apparently narrow spatial and temperature interval in which porphyry deposits form corresponds to a mixing zone between magmatic ore fluids and groundwater (e.g., Hezarkhani et al., 1999). It is argued that dilution of saline magmatic ore fluids by entrainment of groundwater drives precipitation because ligand activity decreases significantly.

The effect of varying salinity on mineral solubility, as might accompany fluid mixing, is readily assessed by examining the shape of the mineral-buffered solubility curves (e.g., Fig. 3a), since such curves directly reflect the relations between total salinity, pH, and dissolved element concentrations. Fig. 7 illustrates mixing relations between Cu-bearing brine and dilute cuprite-saturated fluids, based on the present experiments. Here, the result of mixing is determined by the initial compositions and the relative masses of fluid mixed, and the initial mass of Cpr (if any) in the mixing region. Fig. 7 highlights that copper solubility displays a non-linear, concave down relation between dissolved Cu and Cl concentrations over a wide range of salinity. The form of the solubility curve is such that if fluid-rock chemical equilibrium characterises the zone of fluid mixing then entrainment of heated low-salinity groundwater into a more saline magmatic ore fluid should not result in any significant mineral precipitation, as mixed fluid compositions occurring below the solubility curve on this plot are undersaturated with respect to cuprite. Mixing affects both the ligand and metal concentrations. Moreover, the relation we observe indicates that dissolution of any pre-existing Cu mineralisation in the wall rocks should occur under most mixing conditions. Although probably fortuitous, we note that similar concave down total Cu versus total Cl patterns were calculated by Liu and McPhail (2005) for NaCl–KCl fluids in equilibrium with chalcopyrite + K-feldspar + muscovite + quartz + magnetite + pyrite + pyrrhotite at 400 °C, 50 MPa, supporting our contention that the present results and discussion may have some general applicability to the behaviour Cu in more complex porphyry hydrothermal environments at higher temperatures (>∼500 °C).

Fluid mixing, nonetheless, can trigger mineral precipitation at extreme groundwater/brine ratios and where the final mixture approaches zero-salinity (Fig. 7b). Similarly, it is well appreciated that other factors may also increase

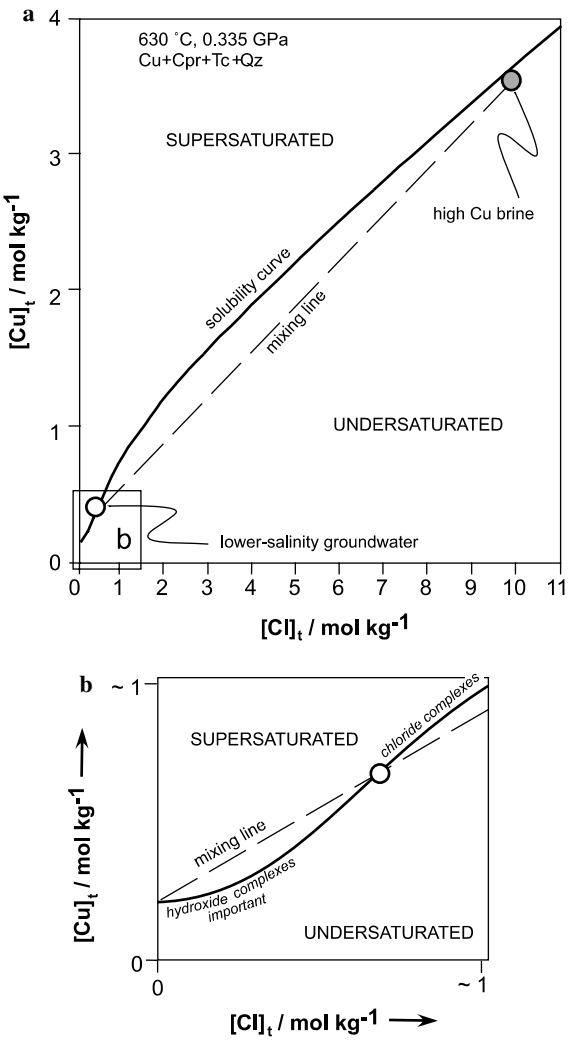

Fig. 7. Simple isobaric, isothermal fluid mixing. (a) Shows the solubility curve (solid line) calculated for Cu + Cpr + Tc + Qz saturated fluid at 630 °C, 0.335 GPa (Table 3) and the effect of fluid mixing (dashed line) between a hypothetical Cu-rich magmatic brine (grey circle) and a cuprite-saturated lower-salinity heated groundwater (open symbol). Fluid compositions occurring below the solubility curve are undersaturated with respect to cuprite, fluid compositions occurring above the solubility curve are supersaturated and metastable with respect to cuprite. (b) Structure of the solubility curve at low salinities (schematic) illustrating the potentially narrow range of composition where fluid mixing can cause cuprite deposition (i.e., supersaturation on mixing) and its expected relation to the transition from copper(I)-chloride to -hydroxide complexes at lower salinity.

the possibility of fluid mixing-induced precipitation (e.g., an ore-bearing fluid mixing with strongly reduced, S-bearing, and/or alkaline groundwaters) as discussed by Liu and McPhail (2005) among others. However, field evidence for fluid mixing occurring above ∼500 °C coupled with the absence of Cu mineralisation at those conditions, suggests such mixing events are rarely witnessed at near-magmatic conditions and that more generally, Cu transport is not readily perturbed by the entrainment of ambient groundwaters at high T (i.e., >∼500 °C).

5.5.2. Fluid cooling: role of higher-order complexes and ore transport

Ore deposition in porphyry Cu deposits occurs, seemingly universally, once T decreases to ~400 °C, and is consistent with the strong decrease in solubility observed in existing experimental data at these lower T conditions. Accordingly, this distinctive feature has been attributed to cooling-induced saturation of the primary ore fluid. However, based on the results of our study, other processes may also lead to mineralisation.

The temperature series data indicates that mineral-buffered solubilities decrease with increasing T (also known as retrograde solubility) above approximately 500 °C, opposite to the trend seen in other lower T experiments. The recognition of isobaric, retrograde mineral-buffered solubilities in low P, high T fluids, e.g., <0.2 GPa, >~500 °C, is not without precedent (e.g., Luce et al., 1985; Grabman and Popp, 1991). We suggested that decreasing solubility with increasing T at isobaric conditions was due to increasing stability of higher order complexes at fixed Cl. In this case, cooling destabilises higher order complexes, liberating HCl to the fluid (raising acidity) which reacts with coexisting minerals (here, cuprite) forming lower coordinated complexes and hence for a constant Cl concentration, results in higher solubilities at lower T. Complex stoichiometry reflects the efficiency of the dissolution process, such that Cl is more efficient in dissolving Cu where the predominant complex has a Cl/Cu of 1 than if this ratio is 4, e.g., $CuCl^0_{(aq)}$ versus $CuCl(HCl)^0_{3(aq)}$. The ligand efficiency decreases at a fixed $[Cl]_t$ with increasing T. Our data provide additional explanation for the apparent absence of Cu mineralised hydrothermal systems above approximately 500 °C and emphasises the potential for transporting ore metals considerable distances (down T) from the source rocks.

5.5.3. Effects of pressure on mineral solubilities in hydrothermal fluids

Simple isothermal decompression causes mineral deposition based on the data presented here. Episodic decompression associated with fracture rupturing and vein formation is common in hydrothermal systems hosted in actively deforming rocks (Sibson, 1987, 1992). Such phenomena, even if unattended by boiling, may be a trigger for mineral deposition in fault zone and fracture networks in medium to high-pressure rocks, e.g., >0.3 GPa.

The effect of pressure on mineral solubility in hydrothermal systems is possibly significant in other respects also. Ultimately fluid decompression leads to liquid–vapour immiscibility or 'boiling'. Despite a paucity of experimental evidence, boiling is often cited as an ore precipitation mechanism (e.g., Cathles, 1977; Henley and McNabb, 1978; Drummond and Ohmoto, 1985; Giggenbach, 1997; Hezarkhani et al., 1999). Whether this is true of porphyry copper systems, however, is not obvious. This is because recent studies of natural coexisting liquid and vapour fluid inclusions (unequivocal evidence of 'boiling') show that Cu (and Au) preferentially partition into the vapour rather the saline brine at some localities (Heinrich et al., 1992; Heinrich et al., 1999; Ulrich et al., 1999, 2001; Heinrich et al., 2004). Our data do not shed additional light on this phenomenon.

General P–T solubility patterns in the present system appear to mimic those observed in the SiO_2–H_2O system (Manning, 1994). The strong pressure dependence also suggests high pressure dehydration reactions associated with subduction of oceanic lithosphere may have a high capacity for extracting Cu (and probably other ore metals) from otherwise refractory phases. Such high-pressure fluids are thought to trigger melting in the mantle wedge beneath magmatic arcs. This may be the primary reason behind the apparent anomalous ore metal enrichment in subduction-derived arc magmas and their associated hydrothermal systems.

6. Conclusions

Experimental solubility data for the mineral assemblage native copper + cuprite + talc + quartz over a wide range of salinity (0.3–11.3 mol kg^{-1} Cl), temperature (525–725 °C), and pressure (0.3–1.7 GPa) were measured. These data can be used to test thermodynamic models of hydrothermal systems at high salinity, pressure and temperature conditions. We infer neutral complexes with the general stoichiometry $CuCl(HCl)^0_{n-1}$ with n up to 4, or so called higher-order complexes ($n > 1$) to be important in these fluids, but note that $n \leqslant 2$ characterises most conditions. Previous experiments have not identified complexes of this type but those studies have been at lower temperature, pressure and salinity conditions.

The data indicate that Cu-Cl complexes are highly stable in mineral-buffered supercritical brine. This results in very high Cu mineral solubilities (wt% concentrations) in brines at magmatic temperatures, such that Cu concentrations required for saturation are probably rarely achieved at such conditions. The shape of the solubility curve over the range of Cl concentration investigated reveals that high temperature mixing between brine and lower salinity fluid is not an important ore depositional mechanism for most groundwater/brine mixtures and is more likely to result in ore/wall rock dissolution. Similarly, above 500 °C solubility trends (in a S-free system) indicate cooling alone will not result in deposition of Cu, whereas below ~500 °C previous work suggests cooling is an effective ore precipitation mechanism. Cu solubility at subduction zone pressures (e.g., ~2 GPa) appears to be extremely high, such that extraction of Cu during slab dehydration is likely to be effective. Solubilities increase with increasing pressure. This pressure sensitivity suggests that episodic decompression, as expected to accompany vein dilation and rupturing in active hydrothermal systems, could be an important ore depositional mechanism irrespective of whether boiling also occurs. Here we investigated the effects of Cl, temperature and pressure on a simple system, constraining the roles of non-equilibrium processes and effects of additional components like Na, K, Fe, CO_2, and S, important in natural hydrothermal environments, will be another decisive step.

Acknowledgments

We wish to thank Bill Hibberson, Dean Scott, and Paul Willis for sharing their experience and help in the high-pressure laboratory at ANU. Mike Shelley and Charlotte Allen are thanked for assistance with LA-ICPMS, Chris Ryan with PIXE, and Andy Christy with quenched solution analyses. Weihua Liu is thanked for helpful discussions and kindly providing access to his own work prior to its publication. Adam Simon and an anonymous reviewer are thanked for their comments on an earlier version of the manuscript. Andrew Berry, Steve Eggins, Jörg Hermann, Hugh O'Neill, and the RSES experimental petrology group are thanked for many constructive discussions. We thank Bob Bodnar and 'Bear' D.C. McPhail for insightful reviews that helped us improve the manuscript. ACH was supported by ANU (Research School of Earth Sciences) through the J.C. Jaeger Scholarship for Ph.D. Research in Earth Sciences.

Associate editor: Liane G. Benning

Appendix A

Logarithm of the equilibrium constant (k) values used in the regression and solubility calculations

°C	525	600	629	650	725	710	710	710	710	
GPa	0.335	0.335	0.335	0.335	0.335	0.313	0.662	0.991	1.703	Source
$1/2Cu_2O_{(Cuprite)} + H^+_{(aq)} = Cu^+_{(aq)} + 1/2H_2O_{(liq)}$	1.9	2.1	2.2	2.3	2.4	2.4	2.6	2.6	2.7	1[a]
$1/3Mg_3Si_4O_{10}(OH)_{2(Talc)} + 2H^+_{(aq)} = 4/3SiO_{2(Quartz)} + Mg^{2+}_{(aq)} + 4/3\ H_2O_{(liq)}$	3.5	3.1	2.9	2.8	2.5	2.6	2.9	3.0	3.2	1[a]
$H^+_{(aq)} + Cl^-_{(aq)} = HCl^0_{(aq)}$	2.1	2.9	3.3	3.5	4.3	4.3	2.6	1.9	1.0	2
$Mg^{2+}_{(aq)} + Cl^-_{(aq)} = MgCl^+_{(aq)}$	2.6	3.6	4.0	4.3	5.2	5.3	2.9	1.9	0.7	3
$MgCl^+_{(aq)} + Cl^-_{(aq)} = MgCl^0_{2(aq)}$	1.3	2.0	2.2	2.4	2.9	2.9	1.6	1.1	0.4	3
$Mg^{2+}_{(aq)} + OH^-_{(aq)} = MgOH^+_{(aq)}$	5.4	6.0	6.2	6.4	7.1	7.0	5.8	5.3	4.7	1
$H^+_{(aq)} + OH^-_{(aq)} = H_2O_{(liq)}$	9.9	10.0	10.1	10.2	10.5	10.5	9.3	8.8	8.2	1
$SiO_{2(Quartz)} = SiO^0_{2(aq)}$	−0.8	−0.6	−0.5	−0.4	−0.3	−0.3	−0.1	−0.1	0.0	4

[a] Mineral properties from Helgeson et al. (1978). 1 = Shock et al. (1997); 2 = Tagirov et al. (1997); 3 = Frantz and Marshall (1982); 4 = Manning (1994). Log_{10} k values above 0.5 GPa were estimated following Manning (1998).

Appendix B

Logarithm of the equilibrium constant (k) values for copper(I) equilibria calculated from Liu and McPhail (2005) and Akinfiev and Zotov (2001) used in solubility calculations

°C	525	600	629	650	725	710	710	710	710
GPa	0.335	0.335	0.335	0.335	0.335	0.313	0.662	0.991	1.703
$1/2Cu_2O_{(Cuprite)} + H^+_{(aq)} = Cu^+_{(aq)} + 1/2H_2O_{(liq)}$	**1.9**	**2.1**	**2.2**	**2.3**	**2.4**	**2.4**	**2.6**	**2.6**	**2.7**
	2.2	2.4	2.5	2.5	2.7	2.7	2.7	2.8	2.8
$Cu^+_{(aq)} + Cl^-_{(aq)} = CuCl^0_{(aq)}$	**3.5**	**3.7**	**3.8**	**3.8**	**4.1**	**4.2**	**3.0**	**2.5**	**1.9**
	2.1	2.3	2.3	2.4	2.6	2.6	1.5	1.1	0.5
$CuCl^0_{(aq)} + Cl^-_{(aq)} = CuCl^-_{2(aq)}$	**1.0**	**1.0**	**1.0**	**1.0**	**1.0**	**1.1**	**0.8**	**0.7**	**0.5**
	3.3	3.5	3.6	3.6	3.8	3.8	3.6	3.5	3.3
$CuCl^-_{2(aq)} + Cl^-_{(aq)} = CuCl^{2-}_{3(aq)}$	**−1.6**	**−1.5**	**−1.5**	**−1.5**	**−1.4**	**−1.4**	**−1.5**	**−1.6**	**−1.6**
	—	—	—	—	—	—	—	—	—
$CuCl^{2-}_{3(aq)} + Cl^-_{(aq)} = CuCl^{3-}_{4(aq)}$	**−0.4**	**0.1**	**0.3**	**0.5**	**1.0**	**0.9**	**1.1**	**1.2**	**1.3**
	—	—	—	—	—	—	—	—	—
$Cu^+_{(aq)} + OH^-_{(aq)} = CuOH^0_{(aq)}$	—	—	—	—	—	—	—	—	—
	6.2	6.9	7.1	7.3	8.1	8.1	6.6	5.9	5.1
$CuOH^0_{(aq)} + OH^-_{(aq)} = Cu(OH)^-_{2(aq)}$	—	—	—	—	—	—	—	—	—
	−2.8	−3.8	−4.2	−4.5	−5.4	−5.1	−5.5	−5.7	−5.9

Notes. Boldface log_{10} k values were calculated from Liu and McPhail (2005) and Cu^+ and Cl^- properties from Shock et al. (1997); plaintext log_{10} k values given directly below were calculated from Akinfiev and Zotov (2001) and use Cu^+ properties from Akinfiev and Zotov (2001), Cl^- and OH^- properties from Shock et al. (1997). Cuprite properties from Helgeson et al. (1978). Log_{10} k values above 0.5 GPa were estimated following Manning (1998).

References

Ahrland, S., Rawthorne, J., 1970. The stability of metal chloride complexes in aqueous solution VII: the chloride complexes copper(I). *Acta Chem. Scand.* **24**, 157–172.

Akinfiev, N.N., Zotov, A.V., 2001. Thermodynamic description of chloride, hydrosulfide, and hydroxo complexes of Ag(I), Cu(I), and Au(I) at temperatures of 25–500 °C and pressures of 1–2000 bar. *Geochem. Int.* **39**, 990–1006.

Archibald, S.M., Migdisov, A.A., Williams-Jones, A.E., 2002. An experimental study of the stability of copper chloride complexes in water vapor at elevated temperatures and pressures. *Geochim. Cosmochim. Acta* **66**, 1611–1619.

Barnes, H.L., 1981. Measuring thermodynamically-interpretable solubilities at high pressures and temperatures. In: Wickman, D.T.A.F.E. (Ed.), *Chemistry and Geochemistry of Solutions at High Pressures and Temperatures*. Pergamon Press, pp. 321–338.

Berry, A.J., Hack, A.C., Mavrogenes, J.A., Newville, M., Sutton, S.R., 2006. A XANES study of Cu speciation in high-temperature brines using synthetic fluid inclusions. American Mineralogist (in press).

Bodnar, R.J. 1989. Synthetic fluid inclusions: A novel technique for experimental water-rock studies. In: Miles, D.L. (Ed.), Proceedings of the 6th International Water-Rock Symposium, A.A. Balkema Publishing Copp. 99–102.

Bodnar, R.J. 1995. Fluid inclusion evidence for a magmatic source for metals in porphyry copper deposits. In: Thompson, J.F.H. (Ed.), Magmas, Fluid and Ore Deposits. Mineralogical Association of Canada Short Course, vol. 23, pp. 139–152.

Bodnar, R.J., Beane, R.E., 1980. Temporal and spatial variations in hydrothermal fluid characteristics during vein filling in pre-ore cover overlying deeply buried porphyry copper-type mineralization at Red Mountain, Arizona. *Econ. Geol.* **75**, 876–893.

Bodnar, R.J., Sterner, S.M., 1987. Synthetic fluid inclusions. In: Ulmer, G.C., Barnes, H.L. (Eds.), *Hydrothermal Experimental Techniques*. Wiley-Interscience, pp. 423–457.

Brimhall, G.H., Crerar, D.A., 1987. Ore fluids: magmatic to supergene. *Rev. Mineral.* **17**, 235–321.

Burnham, C.W., 1979. Magmas and hydrothermal fluids. In: Barnes, H.L. (Ed.), *Geochemistry of Hydrothermal Ore Deposits*. John Wiley and Sons, new york, pp. 71–136.

Candela, P.A., Holland, H.D., 1984. The partitioning of copper and molybdenum between silicate melts and aqueous fluids. *Geochim. Cosmochim. Acta* **48**, 373–380.

Cathles, L.M., 1977. Analysis of cooling of intrusives by groundwater convection which includes boiling. *Econ. Geol.* **72**, 804–826.

Cline, J.S., Bodnar, R.J., 1991. Can economic porphyry copper mineralization be generated by a typical calc-alkaline melt. *J. Geophys. Res. Solid Earth Planets* **96**, 8113–8126.

Crerar, D.A., Barnes, H.L., 1976. Ore solution chemistry. 5. Solubilities of chalcopyrite and chalcocite assemblages in hydrothermal solution at 200° to 350 °C. *Econ. Geol.* **71**, 772–794.

Crerar, D.A., Susak, N.J., Borcsik, M., Schwartz, S., 1978. Solubility of buffer assemblage pyrite + pyrrhotite + magnetite in NaCl solutions from 200 to 350 °C. *Geochim. Cosmochim. Acta* **42**, 1427–1437.

Dilles, J.H., 1987. Petrology of the Yerington Batholith, Nevada: evidence for evolution of porphyry copper ore fluids. *Econ. Geol.* **82**, 1750–1789.

Drummond, S.E., Ohmoto, H., 1985. Chemical evolution and mineral deposition in boiling hydrothermal systems. *Econ. Geol.* **80**, 126–147.

Eastoe, C.J., 1978. Fluid inclusion study of Panguna porphyry copper deposit, Bougainville, Papua New Guinea. *Econ. Geol.* **73**, 721–748.

Eggins, S.M., Kinsley, L.P.J., Shelley, J.M.G., 1998a. Deposition and element fractionation processes during atmospheric pressure laser sampling for analysis by ICP-MS. *Appl. Surf. Sci.* **129**, 278–286.

Eggins, S.M., Rudnick, R.L., McDonough, W.F., 1998b. The composition of peridotites and their minerals: a laser-ablation ICP-MS study. *Earth Planet. Sci. Lett.* **154**, 53–71.

Etminan, H. 1977. Le porphyre cuprifère de Sar Cheshmeh (Iran): Rôle des phases fluides dans les mécanismes d'altération et de minéralisation. In: Sciences de la Terre, Université de Nancy, Mémoires, vol. 34, p. 249.

Frantz, J.D., Marshall, W.L., 1982. Electrical conductances and ionisation constants of calcium chloride and magnesium chloride in aqueous solutions at temperatures to 600 °C and pressures to 4000 bars. *Am. J. Sci.* **282**, 1666–1693.

Fulton, J.L., Hoffmann, M.M., Darab, J.G., 2000a. An X-ray absorption fine structure study of copper(I) chloride coordination structure in water up to 325 °C. *Chem. Phys. Lett.* **330**, 300–308.

Fulton, J.L., Hoffmann, M.M., Darab, J.G., Palmer, B.J., Stern, E.A., 2000b. Copper(I) and copper(II) coordination structure under hydrothermal conditions at 325 °C: An X-ray absorption fine structure and molecular dynamics study. *J. Phys. Chem. A* **104**, 11651–11663.

Fulton, J.L., Chen, Y., Heald, S.M., Balasubramanian, M., 2004. High-pressure, high-temperature X-ray absorption fine structure transmission cell for the study of aqueous ions with low absorption-edge energies. *Rev. Sci. Instrum.* **75**, 5228–5231.

Giggenbach, W.F., 1992. Isotopic shifts in waters from geothermal and volcanic systems along convergent plate boundaries and their origin. *Earth Planet. Sci. Lett.* **113**, 495–510.

Giggenbach, W.F., 1997. The origin and evolution of fluids in magmatic-hydrothermal systems. In: Barnes, H.L. (Ed.), *Geochemistry of Hydrothermal Ore Deposits*, 3rd ed. Wiley-Interscience, pp. 737–796.

Grabman, K.B., Popp, R.K., 1991. Experimental investigation of talc solubility in H_2O–$MgCl_2$–NaCl–HCl fluids in the range 500–700 °C, 2 kb. *Geochim. Cosmochim. Acta* **55**, 2819–2829.

Günther, D., Audétat, A., Frischknecht, R., Heinrich, C.A., 1998. Quantitative analysis of major, minor and trace elements in fluid inclusions using laser ablation inductively coupled plasma mass spectrometry. *J. Anal. At. Spectrom.* **13**, 263–270.

Gustafson, L.B., Hunt, J.P., 1975. Porphyry copper deposit at El Salvador, Chile. *Econ. Geol.* **70**, 857–912.

Hack, A.C., Mavrogenes, J.A., 2006. A cold-sealing capsule design for synthesis of fluid inclusions and other hydrothermal experiments in a piston-cylinder apparatus. *Am. Mineral.* **91**, 203–210.

Harris, A.C., Kamenetsky, V.S., White, N.C., van Achterbergh, E., Ryan, C.G., 2003. Melt inclusions in veins: linking magmas and porphyry Cu deposits. *Science* **302**, 2109–2111.

Hedenquist, J.W., Lowenstern, J.B., 1994. The role of magmas in the formation of hydrothermal ore deposits. *Nature* **370**, 519–527.

Hedenquist, J.W., Simmons, S.F., Giggenbach, W.F., Eldridge, C.S., 1993. White Island, New Zealand, volcanic-hydrothermal system represents the geochemical environment of high-sulfidation Cu and Au ore deposition. *Geology* **21**, 731–734.

Heinrich, C.A., Driesner, T., Stefánsson, A., Seward, T.M., 2004. Magmatic vapor contraction and the transport of gold from the porphyry environment to epithermal ore deposits. *Geology* **32**, 761–764.

Heinrich, C.A., Günther, D., Audétat, A., Ulrich, T., Frischknecht, R., 1999. Metal fractionation between magmatic brine and vapor, determined by microanalysis of fluid inclusions. *Geology* **27**, 755–758.

Heinrich, C.A., Ryan, C.G., Mernagh, T.P., Eadington, P.J., 1992. Segregation of ore metals between magmatic brine and vapor—a fluid inclusion study using PIXE microanalysis. *Econ. Geol.* **87**, 1566–1583.

Helgeson, H.C., 1964. *Complexing and Hydrothermal Ore Deposition*. Pergamon Press, NY.

Helgeson, H.C., 1969. Thermodynamics of hydrothermal systems at elevated temperatures and pressures. *Am. J. Sci.* **267**, 729–804.

Helgeson, H.C., Delany, J.M., Nesbitt, H.W., Bird, D.K., 1978. Summary and critique of the thermodynamic properties of rock-forming minerals. *Am. J. Sci.* **278**, 1–229.

Helgeson, H.C., Kirkham, D.H., Flowers, G.C., 1981. Theoretical prediction of the thermodynamic behavior of aqueous-electrolytes at high-pressures and temperatures. 4. Calculation of activity-coefficients, osmotic coefficients, and apparent molal and standard and relative partial molal properties to 600 °C and 5 kb. *Am. J. Sci.* **281**, 1249–1516.

Hemley, J.J., Cygan, G.L., Fein, J.B., Robinson, G.R., Dangelo, W.M., 1992. Hydrothermal ore-forming processes in the light of studies in rock-buffered systems.1. Iron–copper–zinc–lead sulfide solubility relations. *Econ. Geol.* **87**, 1–22.

Henley, R.W., McNabb, A., 1978. Magmatic vapor plumes and groundwater interaction in porphyry copper emplacement. *Econ. Geol.* **73**, 1–20.

Hezarkhani, A., Williams-Jones, A.E., Gammons, C.H., 1999. Factors controlling copper solubility and chalcopyrite deposition in the Sungun porphyry copper deposit, Iran. *Miner. Deposita* **34**, 770–783.

Holland, H.D., 1972. Granites, solutions, and base metal deposits. *Econ. Geol.* **67**, 281–301.

Holland, T., Powell, R., 1991. A Compensated-Redlich-Kwong (CORK) equation for volumes and fugacities of CO_2 and H_2O in the range 1 bar to 50 kbar and 100–1600 °C. *Contrib. Mineral. Petrol.* **109**, 265–273.

Invernizzi, C., Vityk, M.O., Cello, G., Bodnar, R.J., 1998. Fluid inclusions in high pressure/low temperature rocks from the Calabrian Arc (southern Italy): the burial and exhumation of the subduction-related Diamante–Terranova unit. *J. Metamorph. Geol.* **16**, 247–258.

Johnson, J.W., Oelkers, E.H., Helgeson, H.C., 1992. Supcrt92—A software package for calculating the standard molal thermodynamic properties of minerals, gases, aqueous species, and reactions from 1 bar to 5000 bar and 0 °C to 1000 °C. *Comput. Geosci.* **18**, 899–947.

Keppler, H., Wyllie, P.J., 1991. Partitioning of Cu, Sn, Mo, W, U, and Th between melt and aqueous fluid in the systems haplogranite–H_2O–HCl and haplogranite–H_2O–HF. *Contrib. Mineral. Petrol.* **109**, 139–150.

Liu, W., Brugger, J., McPhail, D.C., Spiccia, L., 2002. A spectrophotometric study of aqueous copper(I)-chloride complexes in LiCl solutions between 100 °C and 250 °C. *Geochim. Cosmochim. Acta* **66**, 3615–3633.

Liu, W., McPhail, D.C., 2005. Thermodynamic properties of copper chloride complexes and copper transport in magmatic-hydrothermal solutions. *Chem. Geol.* **221**, 21–39.

Liu, W., McPhail, D.C., Brugger, J., 2001. An experimental study of copper(I)-chloride and copper(I)-acetate complexing in hydrothermal solutions between 50 °C and 250 °C and vapor-saturated pressure. *Geochim. Cosmochim. Acta* **65**, 2937–2948.

Loucks, R.R., Mavrogenes, J.A., 1999. Gold solubility in supercritical hydrothermal brines measured in synthetic fluid inclusions. *Science* **284**, 2159–2163.

Luce, R.W., Cygan, G.L., Hemley, J.J., Dangelo, W.M., 1985. Some mineral stability relations in the system CaO–MgO–SiO_2–H_2O–HCl. *Geochim. Cosmochim. Acta* **49**, 525–538.

Manning, C.E., 1994. The solubility of quartz in H_2O in the lower crust and upper-mantle. *Geochim. Cosmochim. Acta* **58**, 4831–4839.

Manning, C.E., 1998. Fluid composition at the blueschist—eclogite transition in the model system Na_2O–MgO–Al_2O_3–SiO_2–H_2O–HCl. *Schweiz. Mineral. Petrograph. Mitt.* **78**, 225–242.

Meinert, L.D., Hefton, K.K., Mayes, D., Tasiran, I., 1997. Geology, zonation, and fluid evolution of the big Gossan Cu–Au skarn deposit, Ertsberg district: Irian Jaya. *Econ. Geol. Bull. Soc.* **92**, 509–534.

NBS. 1970. Trace elements in glass SRMs: 610 through 619, inclusive. National Bureau of Standards (certificate), 1–4.

Oelkers, E.H., Helgeson, H.C., 1990. Triple-ion anions and polynuclear complexing in supercritical electrolyte solutions. *Geochim. Cosmochim. Acta* **54**, 727–738.

Oelkers, E.H., Helgeson, H.C., 1991. Calculation of activity coefficients and degrees of formation of neutral ion-pairs in supercritical electrolyte solutions. *Geochim. Cosmochim. Acta* **55**, 1235–1251.

Pearce, N.J.G., Perkins, W.T., Westgate, J.A., Gorton, M.P., Jackson, S.E., Neal, C.R., Chenery, S.P., 1997. A compilation of new and published major and trace element data for NIST SRM 610 and NIST SRM 612 glass reference materials. *Geostandard. Newsl.* **21**, 115–144.

Reynolds, T.J., Beane, R.E., 1985. Evolution of hydrothermal fluid characteristics at the Santa Rita, New Mexico, porphyry copper deposit. *Econ. Geol.* **80**, 1328–1347.

Romberger, S.B., Barnes, H.L., 1970. Ore solution chemistry II. Solubility of CuS in sulfide solutions. *Econ. Geol.* **65**, 901–919.

Rose, A.W., 1970. Zonal relations of wallrock alteration and sulfide distribution at porphyry copper deposits. *Econ. Geol.* **65**, 920–936.

Ruaya, J.R., 1988. Estimation of the instability constants of metal chloride complexes in hydrothermal solutions up to 300 °C. *Geochim. Cosmochim. Acta* **52**, 1983–1996.

Ryabchikov, I.D., Orlova, G.P., Efimov, A.S., Kalenchuk, G.E., 1980. Copper in the system granite-fluid. *Geokhimiya* **9**, 1320–1326.

Sawkins, F.J., Scherkenbach, D.A., 1981. High copper content of fluid inclusions in quartz from Northern Sonora—implications for ore genesis theory. *Geology* **9**, 37–40.

Seyfried, W.E., Ding, K., 1993. The effect of redox on the relative solubilities of copper and iron in Cl-bearing aqueous fluids at elevated temperatures and pressures—an experimental study with application to subseafloor hydrothermal systems. *Geochim. Cosmochim. Acta* **57**, 1905–1917.

Sheppard, S.M., Nielsen, R.L., Taylor, H.P., 1969. Oxygen and hydrogen isotope ratios of clay minerals from porphyry copper deposits. *Econ. Geol.* **64**, 755–777.

Sheppard, S.M., Nielsen, R.L., Taylor, H.P., 1971. Hydrogen and oxygen isotope ratios in minerals from porphyry copper deposits. *Econ. Geol.* **66**, 515–542.

Shock, E.L., Sassani, D.C., Willis, M., Sverjensky, D.A., 1997. Inorganic species in geologic fluids: correlations among standard molal thermodynamic properties of aqueous ions and hydroxide complexes. *Geochim. Cosmochim. Acta* **61**, 907–950.

Sibson, R.H., 1987. Earthquake rupturing as a mineralizing agent in hydrothermal systems. *Geology* **15**, 701–704.

Sibson, R.H., 1992. Implications of fault-valve behavior for rupture nucleation and recurrence. *Tectonophysics* **211**, 283–293.

Sourirajan, S., Kennedy, G.C., 1962. The system H_2O–NaCl at elevated temperatures and pressures. *Am. J. Sci.* **260**, 115–141.

Stefánsson, A., Seward, T.M., 2003. Stability of chloridogold(I) complexes in aqueous solutions from 300 to 600 °C and from 500 to 1800 bar. *Geochim. Cosmochim. Acta* **67**, 4559–4576.

Sterner, S.M., Bodnar, R.J., 1984. Synthetic fluid inclusions in natural quartz. I. Compositional types synthesized and applications to experimental geochemistry. *Geochim. Cosmochim. Acta* **48**, 2659–2668.

Stoffregen, R., 1987. Genesis of acid-sulfate alteration and Au-Cu-Ag mineralization at Summitville, Colorado. *Econ. Geol.* **82**, 1575–1591.

Sverjensky, D.A., Shock, E.L., Helgeson, H.C., 1997. Prediction of the thermodynamic properties of aqueous metal complexes to 1000 °C and 5 kb. *Geochim. Cosmochim. Acta* **61**, 1359–1412.

Tagirov, B.R., Zotov, A.V., Akinfiev, N.N., 1997. Experimental study of dissociation of HCl from 350 to 500 °C and 500 to 2500 bars: Thermodynamic properties of $HCl^0_{(aq)}$. *Geochim. Cosmochim. Acta* **61**, 4267–4280.

Tanger, J.C., Helgeson, H.C., 1988. Calculation of the thermodynamic and transport-properties of aqueous species at high-pressures and temperatures–Revised equations of state for the standard partial molal properties of ions and electrolytes. *Am. J. Sci.* **288**, 19–98.

Ulrich, T., Günther, D., Heinrich, C.A., 1999. Gold concentrations of magmatic brines and the metal budget of porphyry copper deposits. *Nature* **399**, 676–679.

Ulrich, T., Günther, D., Heinrich, C.A., 2001. The evolution of a porphyry Cu–Au deposit, based on LA-ICP-MS analysis of fluid inclusions: Bajo de la Alumbrera, Argentina. *Econ. Geol.* **96**, 1743–1774.

Var'yash, L.N., 1991. Experimental study of Cu(I) complex formation in NaCl solutions at 300 and 350 °C. *Geokhimiya* **8**, 1166–1174.

Var'yash, L.N., Rekharsky, V.I., 1981. Behavior of mono-valent copper in chloride solutions. *Geokhimiya* **7**, 1003–1008.

Walther, J.V., 1997. Determination of activity coefficients of neutral species in supercritical H_2O solutions. *Geochim. Cosmochim. Acta* **61**, 3311–3318.

Williams, T.J., Candela, P.A., Piccoli, P.M., 1995. The partitioning of copper between silicate melts and two-phase aqueous fluids: an experimental investigation at 1 kbar, 800 °C and 0.5 kbar, 850 °C. *Contrib. Mineral. Petrol.* **121**, 388–399.

Xiao, Z.F., Gammons, C.H., Williams-Jones, A.E., 1998. Experimental study of copper(I) chloride complexing in hydrothermal solutions at 40 to 300 °C and saturated water vapor pressure. *Geochim. Cosmochim. Acta* **62**, 2949–2964.